Lasers Technology

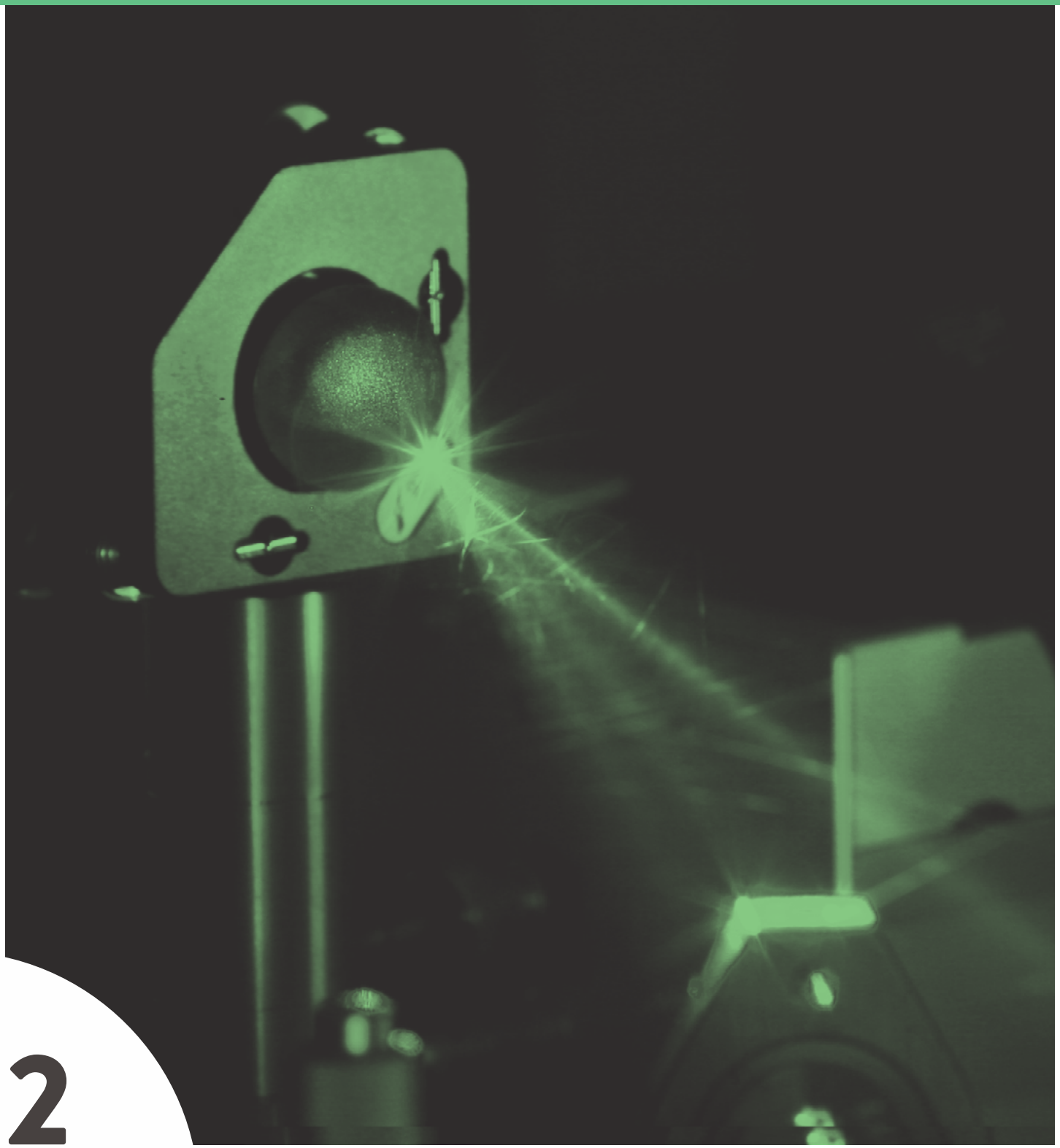

Introduction

The Laser Technology Program of IPEN is located at the Centre for Lasers and Applications (CLA) and is committed to the development of new lasers based on the research of new optical materials and new resonator technologies. Laser application and research occur within several areas such as Nuclear, Medicine, Dentistry, Industry, Environment and Advanced Research. Additional goals of the Program are human resource development and innovation, in association with Brazilian Universities and commercial partners.

The Program is divided into two main areas: "Material and Laser Development" that includes crystal growth of optical materials, characterization, modeling and optical spectroscopy of solids, plasmas and biological materials and the development of compact, highly efficient, diode pumped-solid state lasers.

The other main area, "Laser Applications", is concerned with technological laser uses such as laser processing, laser remote sensing, development of new diagnostic and therapeutic methods such as optical coherence tomography (OCT), laser Doppler flowmetry, photosensitization, prevention of dental caries, medical applications and other advanced applications of high intensity lasers.

One of the biggest labs of the Center for Lasers and Applications uses a terawatt-laser for many of the above applications and also for basic research.

RECENT ACTIVITIES ARE HIGHLIGHTED BELLOW:

1. Development of random lasers at the transition to Anderson localization.
2. Development of cw high power polarized Nd:YAG lasers in fundamental mode operation.
3. Growth of a solid solution $LiGd_{0.232}Lu_{0.75}Nd_{0.018}F_4$:Nd crystal suitable to obtain a laser medium for mode-locking purposes;
4. Characterization, modeling and optical spectroscopy of rare-earth doped crystals and glasses for the development of solid laser medium;
5. First single crystal Nd:YLF fiber laser;
6. Evaluation of the performance of fs laser-induced Breakdown Spectroscopy (fs-LIBS) for the determination of elements in animal tissues.
7. New method for the evaluation of microvascular functionality using low-frequency fluctuations in the laser Doppler flow signal;
8. Skin cancer diagnosis by infrared spectroscopy (FTIR) determining molecular changes in the tissue.
9. Construction of an automatized workstation with ultrashort laser pulses (femtoseconds) for the study of thermal and non-thermal processes in dielectrics, semiconductors and metals;
10. Study of a therapeutic method combining Nd:YAG laser and topical fluoride treatment for effective reduction of caries incidence in patient.
11. Development of studies showing that photodynamic antimicrobial therapy is able to reduce 99% of multi-resistant bacteria in burn wounds.
12. Analysis of Optical Coherent Tomography applied to dermatology (research work winner of the Natura Campus 2010 Premium for Technological Innovation),
13. New LIDAR system for Industrial Emission and Detection installed in Cubatão/SP (collaboration in The National Institutes of Science and Technology Program /INCT).
14. Studies for isotope enrichment by ultrashort laser pulses.

The main activities are based on three pillars: Laser Material Studies, Laser Development and Laser Applications. The development of new laser sources is based on diode pumped solid state lasers (DPSSL) for applications in research, industry, medical and pollution control. Our investigations are focused mainly on controlling the temporal, spectral and spatial features of the laser beam. In some cases, it also includes the production design of such systems including the reliability tests and application experiments. We have built several DPSSL systems emitting from the blue up to the far infrared.

We have developed several proprietary designs, the most important being called DBMC (double-beam mode controlling), that has resulted in extremely efficient and compact diode-laser with up to several tens of watts of output power in continuous (cw) operation. Some highlights of the last period are shown below:

- We built several DPSSL Raman lasers that resulted in either never before reported laser lines or, a very compact design, not needing the fiber-coupled diode lasers. For example, the first compact side-pumped DPSSL Nd:YVO self - Raman laser, operating at 1176 nm and 589 nm. Also, the first three-level Nd:YLF/KGW Raman laser operating at 979 nm and 990 nm. A highlight in terms of Raman lasers was a intracavity frequency converted three level Nd:YLF/KGW Raman laser generating 10 laser lines in the deep blue to cyan spectral region with up to 1 W of output power.

- The highest efficiencies for diode pumped Nd:YLF lasers reported so far were achieved: more than 60% at 1053 nm in a side pumped configuration in qcw operation, but also at 1313 nm and in Q-switched operation.

- We started to build highly efficient, dynamically stable, cw high power lasers with up to 60 W output power, 60% TEM_{00} extraction efficiency and high misalignment stability, based on OEM diode-pumped Nd:YAG modules.

- We are also researching random laser light sources that are used in optofluidic devices for real-time system control and quantitative analysis of important process parameters (Figure 1). One laser source, using a hollow-core antiresonant reflecting optical waveguide (HC-ARROW) containing the gain media inside a reservoir to reduce dye bleaching, is connected to microchannel waveguides to increase beam directionality. The device, which is pumped externally, emits a highly coherent and collimated laser beam of only 68 mrad divergence (Figure 1).

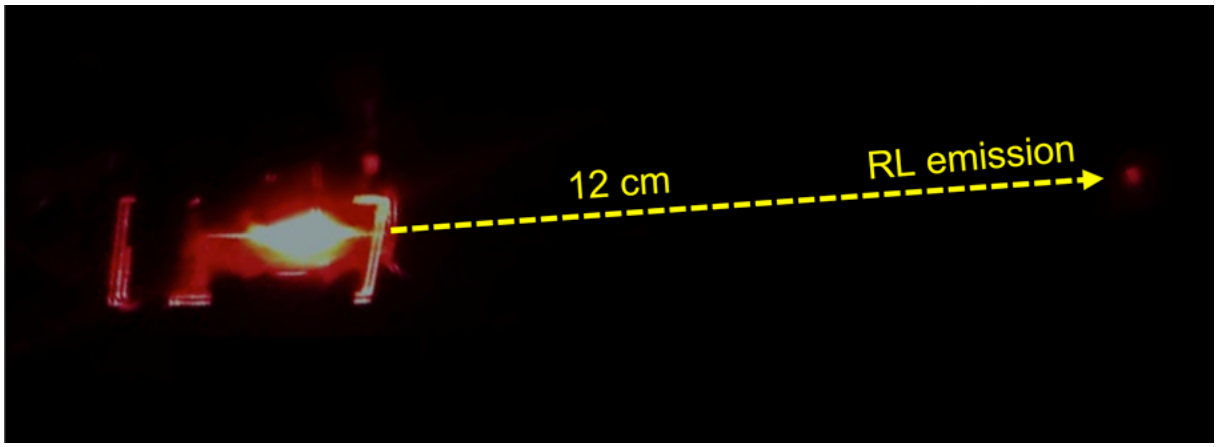

Fig 1: Directional Random Laser in action

- We also report resonant feedback random lasing from dye-doped biopolymer films, consisting of a deoxyribonucleic acid-cetyltrimethylammonium (DNA-CTMA) complex doped with DCM dye. The interesting feature about this random laser is that it works with a spatially localized feedback much alike a standard laser (Figure 2).

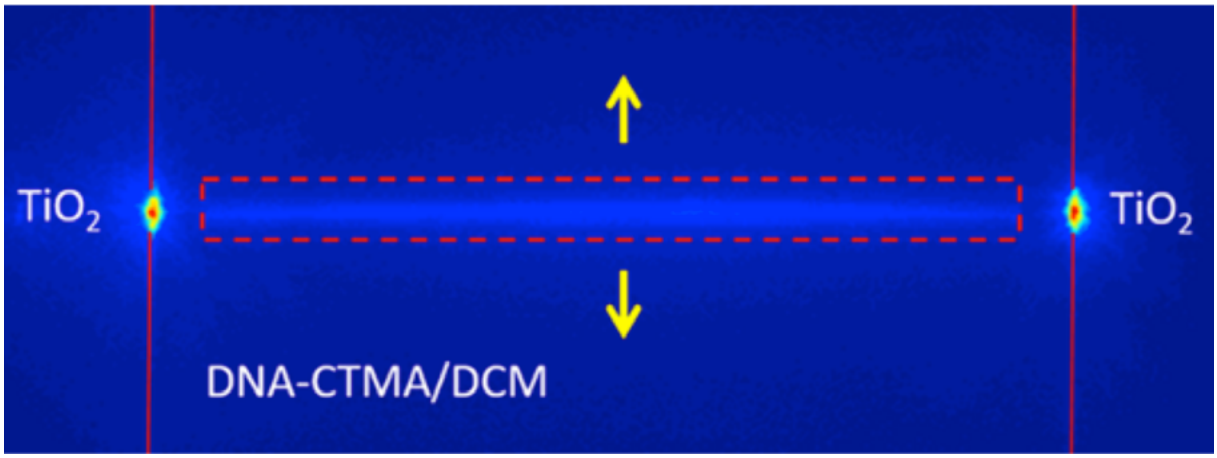

Fig 2 – Laser Resonator Schematics made of DNA

- We report an alternative experimental setup to laterally focus light at an angle of 90 deg relative to turbid, multiple scattering media, using preprocessing wavefront shaping. We compare the measured image quality to one obtained in the usual configuration for focusing light through turbid media, where focusing occurs behind the scattering sample. We demonstrate that the depth of focus in the lateral configuration is of the same order of the usual transversal one because both setups are designed to operate in the deep Fresnel zone. This result shows that this novel, versatile lateral configuration allows for effectively focusing around corners through multiple scattering samples.

In order to obtain these lasers, the growth of crystal is an important activity in our center. Single crystal fibers are known as a low cost and reduced dimension alternative for laser devices and an ideal method for crystallization studies. Fiber crystals are also particularly well suited for wave-guiding in the IR region, tunable narrow-band filters and nonlinear optics due to their long interaction length and tight beam confinement.

Rare earth doped tungstate single crystals have early gained attention because of their suitable properties for laser media application. However, many of the tungstate compounds undergo phase transitions and they cannot be grown directly from their melts. Among the tungstate crystals, the compound $LiLa(WO_4)_2$ is one that have (has) a relatively low melting point (1065 °C) and no phase transitions upon cooling. We investigated the growth process of Er^{3+}/Yb^{3+}:$LiLa(WO_4)_2$ single crystal fibers by the micro-pulling down method. The material's synthesis by solid-state reaction and the effect of different dopant concentrations on the melting properties were studied. The addition of Yb modifies the melting behavior of this compound and $LiLa_{(1-x)}Yb_{(x)}(WO_4)_2$ single crystal fibers can be grown up to limited Yb concentrations. Single crystal fibers with 1 mm in diameter

and 10mm long were prepared with fixed Er concentration (0.5 mol%) and 1, 2, 5, 7 and 10 mol% of Yb.

Because of the suitable optical properties of alkaline-earth fluorides - CaF_2, SrF_2, BaF_2, MgF_2, MnF_2, this family of crystals, in particular the CaF_2, is commonly used to build commercial optics and devices in the ultraviolet as well as in the infrared spectral domain. They also found application also as laser hosts. The growth of BaF_2 single crystal fibers, doped with rare earth ions (Pr^{3+}, Tm^{3+}) for spectroscopic studies aiming to the development of compact laser systems, was performed (Figure 3). The equilibrium of thermal conditions for the pulling of regular and homogeneous BaF_2 single crystal fibers was defined for the micro pulling down technique on resistive mode. The effect of the atmosphere (Ar/CF_4), and, the appropriate mixture balance to assure the reactive atmosphere efficiency and the appropriate capillary stability were determined empirically. The dopant distribution and their influence on the optical and structural quality of the growth of the fluoride single crystal fiber are under investigation (Figure 4).

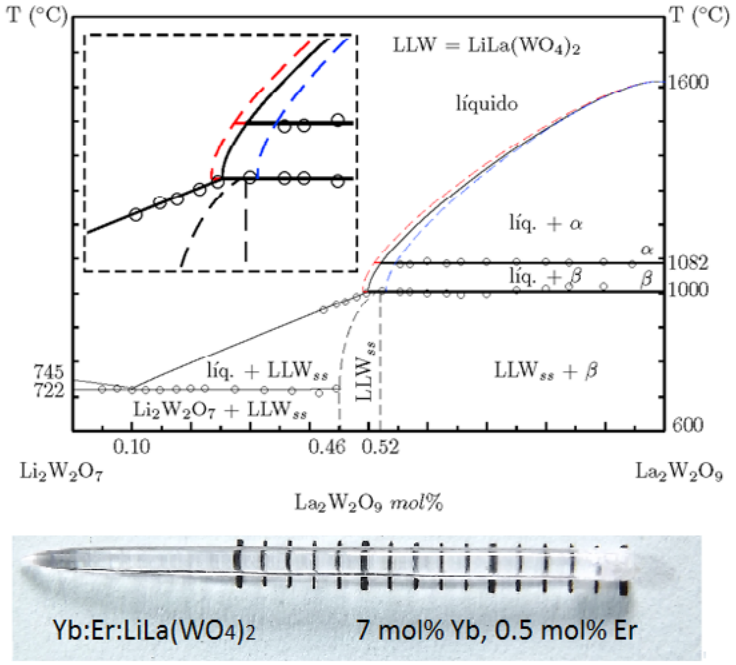

Fig 3 – Experimental equilibrium phase diagram of quasi-binary system $Li_2W_2O_7$ – $La_2W_2O_9$ studied at CLA and doped single crystal fibers obtained from this data. $LiLa(WO_4)_2$ is formed at x = 0.52 and decomposes peritetically at 1000°C. The dashed lines describe the influence on the liquidus by doping with Gd (red) and Yb (blue).

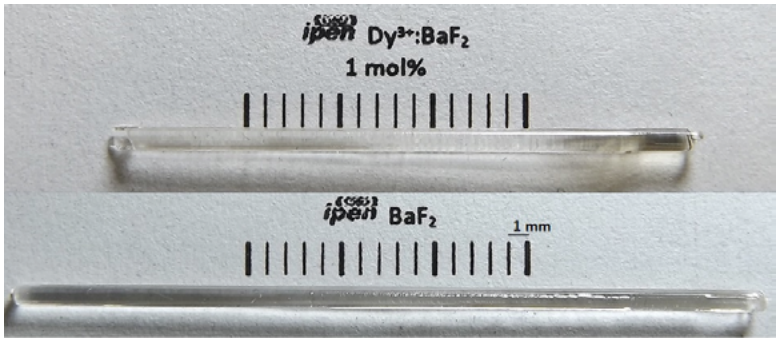

Fig 4 –BaF_2 single crystal fibers grown by micro-pulling down method.

Crystal growth activities

Recently, rare earth doped nanocrystals received great attention due to their application in high-resolution panels, integrated optical systems and biological labeling. The controlled synthesis of nanoparticles with uniform size, shape, structure and rare earth doping became of fundamental importance once the final properties are directly related to these parameters.

The $NaYF_4$ is a very efficient host matrix for trivalent rare earth ions such as Yb/Er and Yb/Tm for up-conversion systems. There are several synthetic processes already reported in the literature for production of this material, involving different chemical routes and processing from organic and inorganic compounds, however, the reproducibility of these processes are not always achieved. We are studying the production of $NaYF_4$ co-doped with Yb^{3+}/Er^{3+} by micro-flow reaction using a microchannel system. A microfluidic circuit was designed and fabricated at the Center for Lasers and Applications at IPEN. It is a two-stage microfluidic reactor - in the first stage, the product stream (NaF solution) is combined with the second precursor stream ($RECl_3$ solution, were RE = rare earth). In the second stage, the compounds flow through a heated zone (temperature range of 70 - 100°C). The main compounds are guided through the system with two syringes, with flow controlled by the applied pressure (electronic controlled). Experiments are under way to analyze injection flow rates of the components, aiming to define the residence rate and temperature for desired nanoparticles production.

The next step before laser development is the characterization, modeling and optical spectroscopy of rare-earth doped solid laser media. A luminescence spectroscopic system with spectral and temporal discrimination that uses a Box-car technique and tuneable laser excitations of 4 ns (10 Hz) in the range of 420 to 2000 nm (10mJ) was used for lifetime measurements of rare earth ions in glasses and fluorides crystals. These measurements allowed determining the rate constant of the non-radiative energy transfer that happens due to multipolar interactions between donor and acceptor ions in solids. Energy transfer mechanism involving two interacting erbium (and holmium) ions in the first (and second) excited state, energy-transfer up-conversion have (has) been observed and the rate constant determined. The aim of this study is the development of solid laser medium emitting in the mid-infrared (2700 - 3600 nm) and to improve the small signal gain laser emission of Er^{3+} and Ho^{3+}-doped materials. A detailed investigation of the energy transfer processes involving one or two excited Ho^{3+} ions in Ho^{3+}-doped InF_3 glass has been performed to examine all the energy transfer rates relevant to the $^5I_5 \rightarrow {}^5I_6$ transition at 3930 nm as a function of the Ho^{3+} concentration (2, 4 and 10 mol %). The decay times, branching ratios and rate parameters for the energy transfer, were measured and they were used as the input parameters for a rate equations analysis. Excited state absorption (ESA) initiating from the lower laser level of Ho^{3+} was determined in this study. Numerical simulation of CW laser emission at 3930 nm was performed using two pump wavelength, one for the upper laser level excitation (i.e. $^5I_8 \rightarrow {}^5I_5 = \lambda_{P1}$) and the other for lower laser level de-excitation (i.e. $^5I6 \rightarrow {}^5S_2 = \lambda_{P2}$). The pump wavelength λ_{P1} = 889 nm was chosen to match the fundamental absorption of the $^5I_8 \rightarrow {}^5I_5$ Ho^{3+} transition and the pump wavelength λ_{P2} = 962 nm was determined based on the measurements of ESA and the application of the McCumber method. Critically, the estimated ESA

cross-section at λ_{P2} – 962 nm is approximately sixteen times larger than the ground state ($^5I_8$) absorption process. Our calculation suggest(s) that even for high Ho^{3+} concentration in which cross-relaxation has been shown in previously to quench the $^5I_6$ level, ESA is nevertheless strong enough to allow a sufficient population inversion required for practical CW laser emission at 3930 nm. A Ho^{3+} -doped InF3 glass with holmium concentration of 10 mol% can be used as a practical laser medium to generate continuous laser emission at 3930 nm using two diode lasers pumping at 889 and 962 nm.

Laser applications

The laser applications are focused on 4 main areas: Industrial, Health, Nuclear and Environmental. The processing of materials with ultra-short laser pulses (in the order of 10^{-13} to 10^{-14} s) has been developed in the Center of Lasers and Applications both for the understanding of the physics interaction of this type of laser with the matter as for its use in practical applications. Unlike other types of lasers, ultra-short pulses can process structures virtually free of thermal effects. This enables the machining of extremely small structures without burrs, resolidified material or heat affected zone. Using such technique, very tiny structures have been produced on several kinds of materials such as glasses, metals and polymers. In polymers, very narrow and very close grooves (~ 10 microns) are being produced and used for alignment of cells for growth of specific biological tissues. In metals, a color-forming technique has been developed on its surface without the formation of coating layers such as oxides or nitrides, preserving to the maximum its physical and metallurgical properties. In addition to colorization, highly light-absorbing structures were produced on metal surfaces, with an absorption rate above 95% for the visible and near infrared regions. Also, micrometric textures are being developed in metals with the purpose of improving the tribological properties of their surfaces. These textures can reduce the friction and wear of surfaces used in numerous engineering processes.

The glass processing with ultra-short femtosecond pulses has been developed and is being used mainly for the production of components for microfluidic circuits. Micro channels, micro reactors, valves and micro pumps are some of the regularly produced components. With them, several complete microfluidic circuits were produced, including the injection and control systems (Figure 5). The main circuits already in operation are being used for ELISA assay (Enzyme Linked Immuno Sorbent Assay), for the growth of luminescent nanocrystals and for the control of size and shape of metallic nanoparticles.

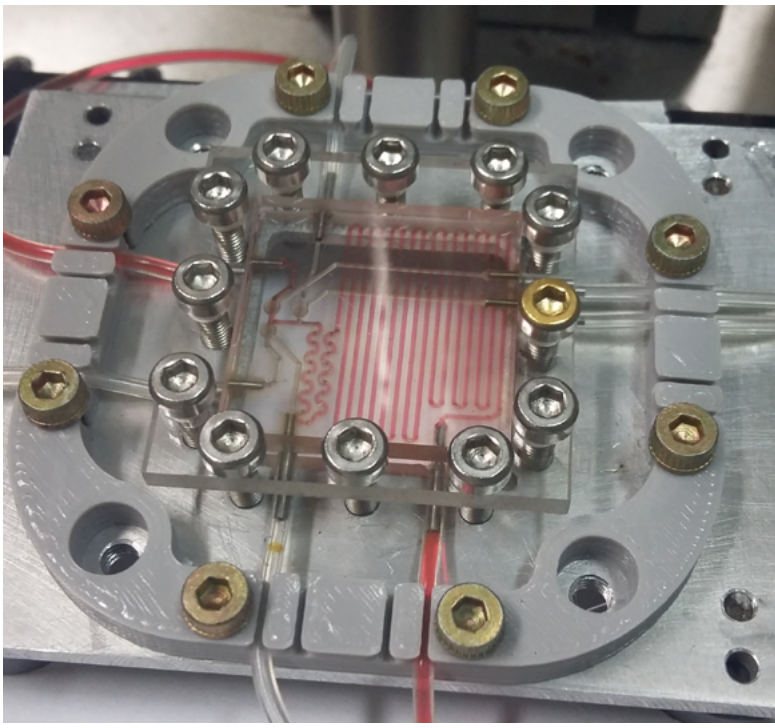

Fig 5 -Microfluidic system for growth of luminescent nanocrystals.

Laser Applications in Health Sciences

Biophotonics is an exciting interdisciplinary research field which studies the interaction of photons with biological structures, imaging and sensing cells and tissue. The interaction of light with matter results in reflection, absorption, scattering or transmission of the beam which can tell us information about the molecule or tissue structure. Since 1992, Biophotonics and lasers research at IPEN is providing to the society with a wide range of applications from fundamental medical research to diagnosis, therapy and surgery.

Diagnosis of skin cancer

Nonmelanoma skin cancers represent 95% of cutaneous neoplasms. Among them, squamous cell carcinoma (SCC) is the more aggressive form and shows a pattern of possible metastatic profile.

5-aminolevulinic acid (ALA) and its methylated ester (MAL) are the most common topical agents used in photodynamic therapy (PDT) as precursors of the photosensitizer protoporphyrin IX (PpIX). The induction of newly PpIX depends on incubation time of each photosensitizer in the tissue and the presence of high intralesional porphyrin levels is an important parameter for the PDT effectiveness. We used laser-induced fluorescence (LIF) spectroscopy to evaluate the optimum time to light exposure of PDT mediated by ALA (20% w/w) and MAL (10% w/w) to treat malignant lesions precursors of cutaneous squamous cell carcinoma induced in mice. The therapeutic effects obtained by optimized ALA- and MAL-PDT were assessed 10 and 20 days after treatments. Higher PpIX levels were evidenced in the lesions photosensitized by ALA than MAL and according to LIF measurements the PDT irradiation was performed, respectively, at 300 and 330 minutes after ALA and MAL incubation. Histopathological analysis evidenced necrosis and epithelial atrophy after 10 days of PDT using both prodrugs, as well as reepitelization and collagen deposition at 20 days. Thus, despite the distinct concentration of ALA and MAL used in the formulation of each photosensitizing cream, PDT mediated by both photosensitizing agents obtained similar therapeutic outcomes. Besides, we used Fourier transform infrared spectroscopy (FTIR) spectroscopy to assess the biochemical changes in normal skin caused by squamous cell carcinoma induced by multi-stage chemical carcinogenesis in mice. Changes in the absorption intensities and shifts were observed in the vibrational modes associated to proteins, indicating changes in secondary conformation in the neoplastic tissue. Hierarchical cluster analysis was performed to evaluate the potential of the technique to differentiate the spectra of neoplastic and normal skin tissue, so that the accuracy obtained for this classification was 86.4% (Figure 6).

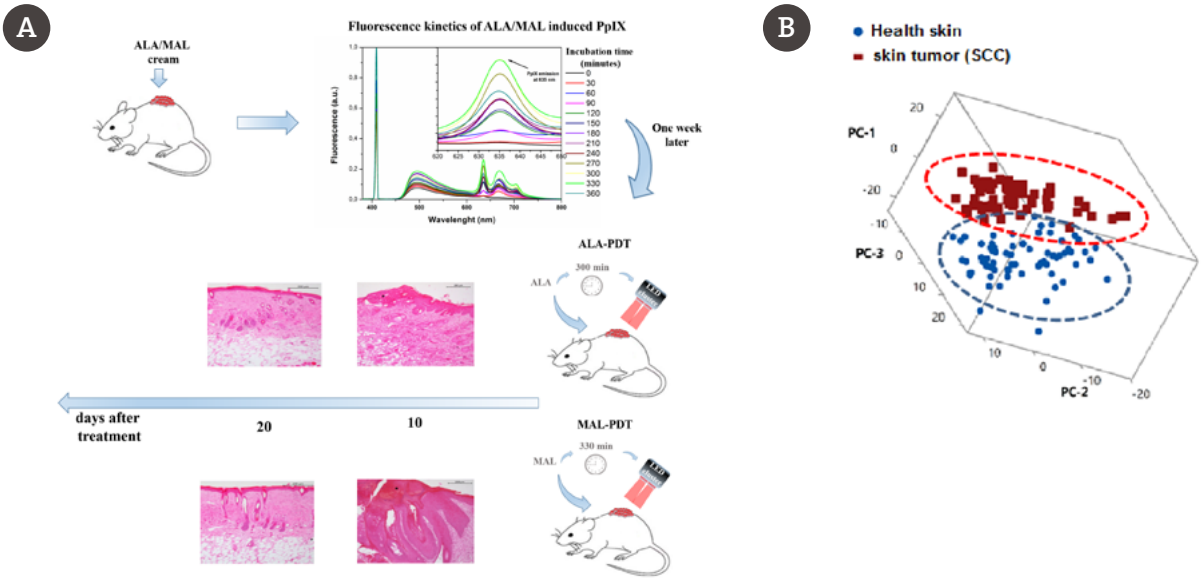

Figure 6: (a) Illustration of fluorescence from skin tumor treated by PDT mediated by ALA and MAL and histological results. (b) Discrimination of healthy and skin tumor by multivariate statistical analysis.

Photodynamic therapy of skin cancer

Photodynamic therapy (PDT) has become a promising alternative for treatment of skin lesions such as squamous cell carcinoma. We propose a non-invasive method to monitor the effects of PDT by using the optical attenuation coefficient (OAC) calculated from optical coherence tomography (OCT) images. We conducted a study on mice with chemically induced neoplastic lesions and performed PDT on these lesions using local developed photosensitizers cream (PI 0705591-9). The response of neoplastic lesions to therapy was monitored using, at the same time, macroscopic clinical visualization, histopathological analysis, OCT imaging, and OCT-based attenuation coefficient measurement. Results with all four modalities demonstrated a positive response to treatment. The attenuation coefficient was found to be 1.4 higher in skin lesions than in healthy tissue and it decreased after therapy, demonstrating that the OAC is a potential tool to noninvasively assess the evolution of skin neoplastic lesions with time after treatment.

Effects of ionizing radiation (Co^{60}) on biological hard tissues

Ionizing radiations, such as X-ray or Gamma radiation, are well-recognized as effective treatment and diagnostic methods for malignant diseases, as well as for sterilization of tissues. However, these radiations can chemically alter the target tissue, and these changes can affect morphology, crystallinity, healing and mechanical properties of irradiated tissues, mainly considering enamel, dentin and bone. Bone samples were irradiate with 0.01 kGy, 0.1 Gy and 1kGy a Co^{60} Gammacell irradiator (1.43 kGy/h) while the irradiations with 15kGy and 75kGy were performed at Co^{60} multipropose irradiator (6.0 kGy/h). ATR-FTIR spectroscopy analysis showed a significant change on the amide II band (1580-1480 cm^{-1}), which indicates that gamma radiation induced changes on helical structure of collagen, and these changes have a direct relation with the dose, however it does not interfere in the inorganic matrix of bone, since the content of carbonate was not altered after gamma irradiation. The crystallinity index is useful for evaluating the order, organization and tension of the hydroxyapatite crystals. Crystal growth and crystallinity of hard tissues can be affected by factors such as the maturity degree of tissue or even due to the increase on its temperature. Our results evidenced that low doses of gamma radiation (0.01 kGy) decreases the crystallinity of bone; however doses higher than 0.1 kGy, did not promote significant changes on the crystallinity index when compared to the non-irradiated samples. In this way, we can infer that low doses of gamma radiation have a significant effect on the crystal characteristics of hydroxyapatite from the bone and this effect, together with the effect on collagen secondary structure, can be the main reason for the changes on the mechanical properties on sterilized bone showed on literature.

Prevention of dental caries with lasers

Dental caries are a common oral disease which, viewed simply, is characterized by a demineralization of the dental hard tissue caused by acids generated in the oral biofilm. Although a remarkable decline in the incidence of dental caries worldwide has been documented, it is still the most prevalent disease during childhood and adolescence. On account of the widespread use of fluoride, lasers have been tested to improve dental enamel properties in order to enhance its resistance to demineralization. We evaluated the effect of combining laser irradiation (Nd:YAG and Er,Cr:YSGG) with fluoride on an enamel microstructure and de-

mineralization by FTRaman spectroscopy. Demineralization promoted reduction in organic contents; Nd:YAG laser irradiation promoted loss of carbonate and organic content, while Er,Cr:YSGG did not produce significant changes in the relative band intensities of organic and inorganic contents of the enamel. In lased samples, no effects caused by pH-cycling on enamel were observed. Our group showed that laser treatment and its association with fluoride can interfere with the demineralization dynamics, reducing its effects over the enamel.

Lasers cutting bone and dental hard tissues

Infrared lasers can be useful in several applications, since they are strongly absorbed by water and hydroxyapatite, two of the main components of the body mineralized tissues, like enamel, dentine and bone. The Er,Cr:YSGG laser (2780 nm) cuts bone by thermal ablation. In this process, the water molecules of tissue absorb the laser energy, increasing its temperature and the pressure inside the tissue, causing a micro-explosion that removes the material. However, for an efficient and safe application, it is necessary to know the exact effects that the laser irradiation promotes in tissue. Infrared Thermography and Attenuated Total Reflectance-Fourier Transform Infrared spectroscopy (ATR-FTIR) techniques were used to characterize natural and irradiated bone tissue showing that irradiation at 3 J/cm^2 promotes an increased temperature of approximately 100 °C, while 6 J/cm^2 up to 215 °C; 8, 12, and 15 J/cm^2 promoted increased temperature up to 300 °C. The compositional analysis revealed that laser irradiation promotes changes in the carbonate content and affects the intermolecular interaction within the mineral part of bone. Moreover, the proportion of organic components (amides) in the bone samples significantly decreased with the increase in energy density, which points out the importance of using the proper energy density in clinical procedures to avoid thermal or chemical damage to the tissue caused by laser irradiation.

Other Laser Health activities (activities) include Development of therapeutic processes of photobiomodulation and photodynamic inactivation which aims to explore innovative light-based therapeutic processes through low power lasers and light-emitting diodes (LEDs) to provide scientific background for clinicians. Our major interests are to investigate the effects of photobiomodulation (PBM) and photodynamic inactivation (PDI) therapies. Other activities encompass tissue optics, nanomaterials, and tissue engineering.

Photobiomodulation

Photobiomodulation (PBM) is a non-invasive therapeutic modality used in Health Sciences for pain relief, wound healing, bone repair, although mechanisms behind its effects are still not completely known. Our group develops researches about the physical, chemical and biological mechanisms of the non-thermal effects of light on biological tissues. Studies are carried out in vitro and in vivo to investigate the influence of PBM on cell cultures, tumor cells, pain relief, bone repair, and chronic inflammation in obesity. Our results show that PBM is able to trigger senescence in tumor cells, but proliferation in fibroblasts following gamma-radiation, reduces abdominal adipose tissue inflammatory infiltrate of diet-induced obese and hyperglycemic mice, stimulates bone metabolism and inhibits root resorption during tooth movement in rodents, and modulate serotonin levels and blood flow in women with headache. Skin optics changes, depending on mouse gender and strain suggesting that absorption and scattering

coefficients, should be considered to optimize light-based therapy and diagnosis (Figure 7).

Photodynamic inactivation (PDI) is a promising therapeutic approach that involves the use of a photosensitizer, a light source, and oxygen

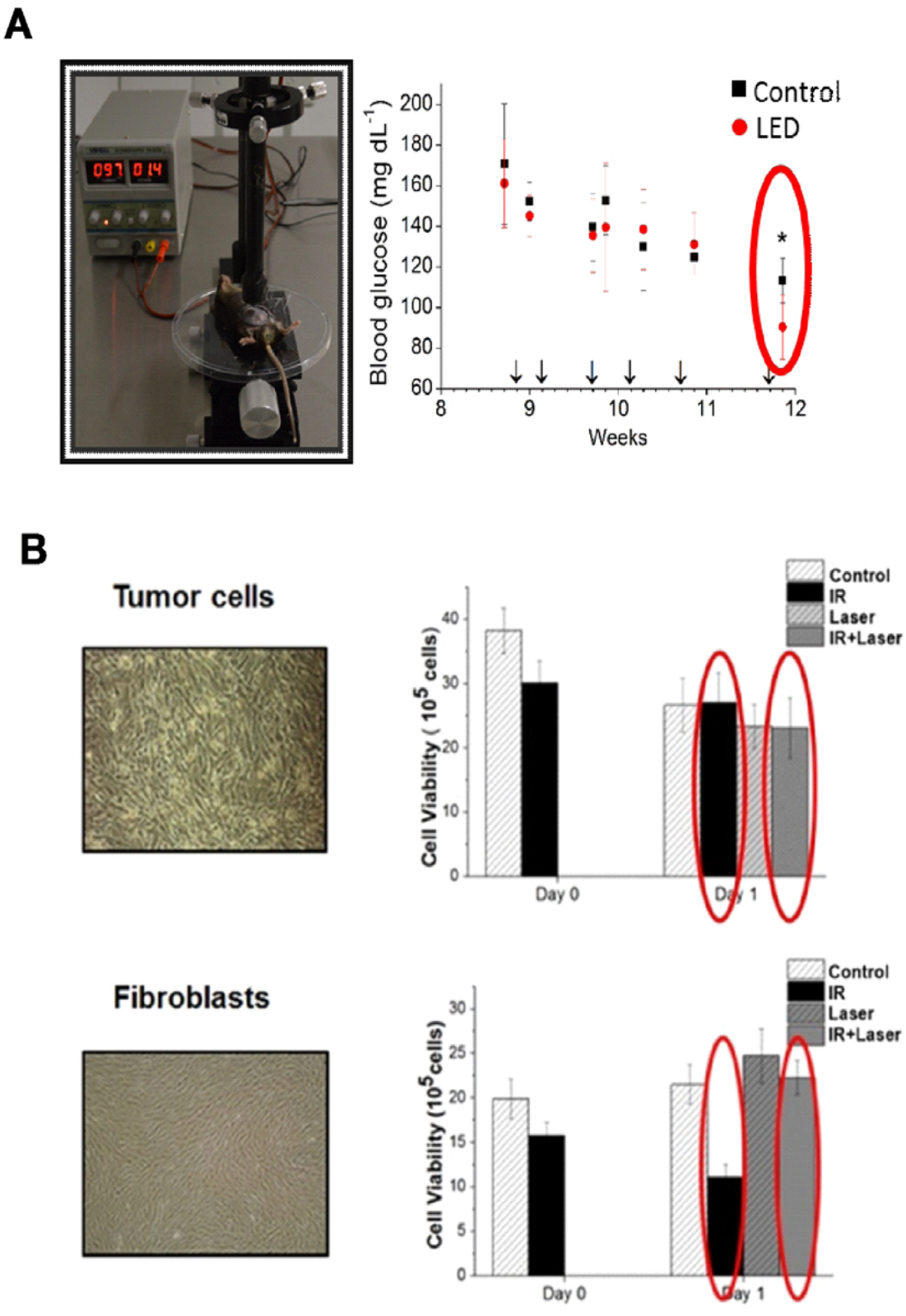

Figure 7: Photobiomodulation therapy decreases glucose in blood of obese mice (A) and does not proliferate tumor cells (B).

to kill bacteria, fungi, viruses, and protozoa, including those resistant to conventional drugs. Alone, neither photosensitizer nor light produce damage in infected tissues. Studies are performed in vitro and in vivo to investigate mechanisms and optimize PDI. Our results show that PDI predominates on different targets depending on cell growth phase. It can be enhanced by glucose and urea through different mechanisms , and induces programmed cell death in protozoa, which contributes to reduce lesion size, parasite load and pain in Leishmania amazonensis-induced cutaneous leishmaniasis in mice. Besides, we designed a dedicated light source to decontaminate biomedical instruments. In Veterinary Medicine, PDI proved to be an alternative treatment for caseous lymphadenitis abscesses in sheeps and footpad dermatitis in penguins (Figure 8).

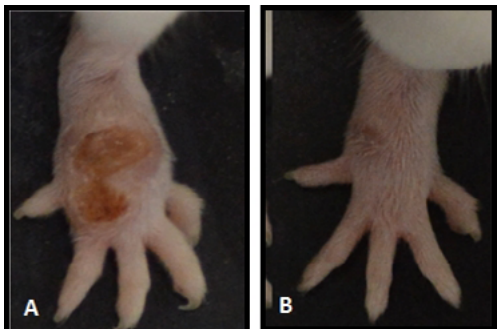

Figure 8: Photodynamic inactivation accelerates wound healing and reduces parasite load in cutaneous leishmaniasis induced in paw of mice. A: control lesion without treatment; B: lesion treated after 4 weeks.

A Microfluidic device for ELISA assay was produced with ultra-short laser pulses micromachining on BK7 optical glass as a proof of concept for ELISA assay. The device can be used to prove the presence of the most diverse antigens. Figure 9 shows the first circuit of this type produced in the CLA-IPEN that was used with jararaca antigen.

In this case, the microreactor of the circuit is sensitized with jararaca antigen and subsequently washed with TBS (tris-buffered saline, pH8) to remove non-adsorbed antigen. Then, a blocking solution is injected with the purpose is of adhering in spaces of the channel where the antigen did not adhere. The entire loop is then washed again with TBS and inoculated with primary antibody and subsequently with the secondary antibody, and finally washed again. A colorimetric reaction is produced in the microreactor to indicate the presence of the antibody. The use of the development kit whose substrate is orthophenylenediamine showed a color change from transparent to yellowish, evidencing the success of the device produced. Assays on plaques without the antigen were also made for the negative control.

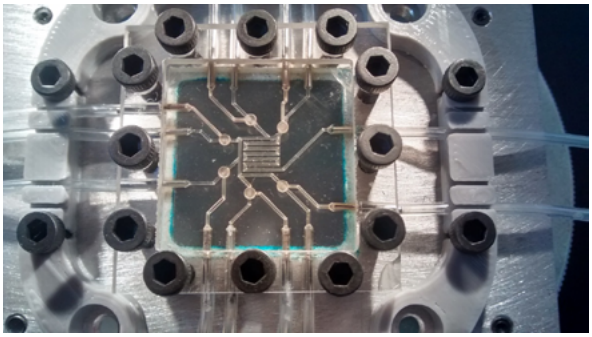

Figure 9: Microfluidic circuit used for ELISA. The microreactor is the central serpentine.

As a diagnostic tool another laser health application Optical coherence tomography (OCT) is a diagnostic imaging technology based on low length coherence interferometry in which the coherence features of photons are explored, leading to an imaging technology that is capable of producing non-contact, non-destructive, high-resolution cross-sectional images of internal microstructures of living tissues. We implemented several OCT systems.

Innovative studies are being performed in order to make OCT a tool more powerful and flexible. The laboratory has studied the improvement of optical setup itself and also new ways of data analysis, such work provided interesting results in the period, and they are

presented in the following paragraphs.

A non-invasive technique for glucose monitoring was developed in order to improve glucose control and treatment in patients with diabetes. Optical Coherence Tomography may offer a good alternative for portable glucometers, since it uses light to probe samples. Changes in the object of interest can alter the intensity of light returning from the sample and, evaluating these changes, one can estimate the sample's attenuation coefficient (μt) of light. We explored this behavior of μt for mouse's blood under increasing glucose concentrations. The system proved to be sensitive for all blood glucose concentrations tested, with good correlations with the obtained attenuation coefficients. A linear tendency was observed as a function of increasing attenuation with higher values of glucose. Statistical difference was observed between all groups ($p<0.001$). This work opens the possibility towards a non-invasive diagnostic modality (Figure 10).

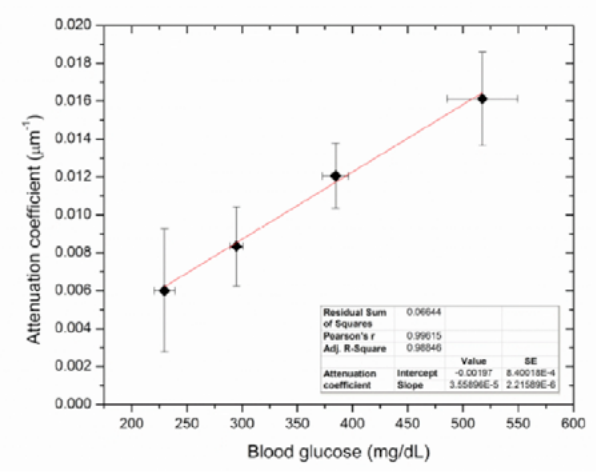

Figure 10: Attenuation coefficients calculated in relation to average blood glucose concentrations, after refractive index correction (IR=1.26). Multiple comparison analysis showed $p<0.001$ between every group (Kruskall-Wallis with Dunn's as post hoc). Red line represents the best linear correlation obtained, with slope of 3,55e-5 with an adjusted R-Squared of 0.98, which indicates that a linear model is suitable for our data.

The laboratory also has proposed a new methodology which uses OCT to Particle size and morphological characterization of cosmetic emulsified systems. The physicochemical attributes of emulsified systems are influenced by the characteristics of their internal phase droplets (concentration, size and morphology), which can be modified not only by the formulation components, but also by the analytical methodology employed. Thus, the physicochemical characterization of cosmetic emulsions obtained from different surfactants , was made with OCT as the analytical technique employed for the morphological characterization and particle size determination of the formulations. Three emulsions were prepared, differing at the type and concentration of the surfactant used, and their droplet sizes were evaluated (Figure 11).

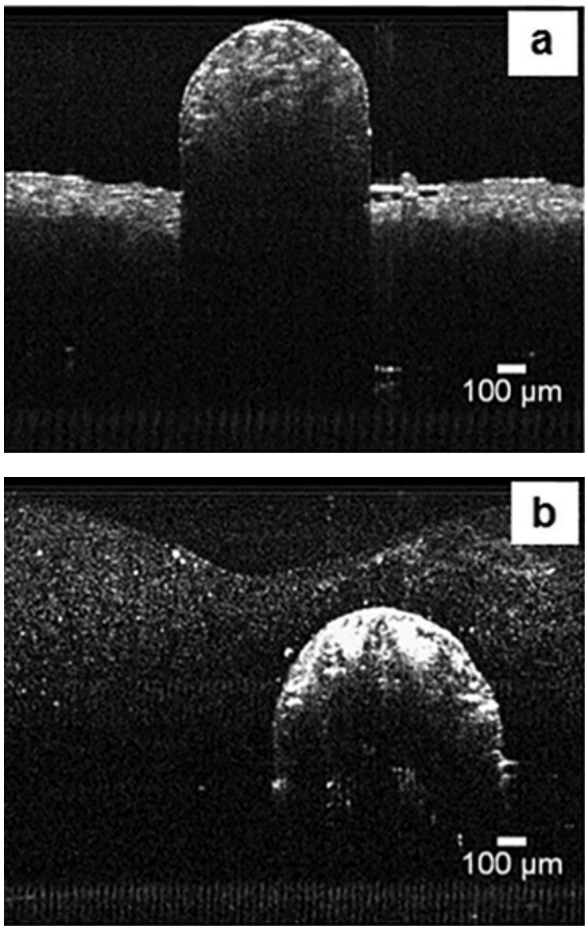

Fig. 11 - Microspheres and carbomer gel 1.0% (w/w), (a) sphere above the carbomer gel and (b) sphere within the carbomer gel.

Another interesting case was the work in

which it was possible to evaluate the progression of erosive lesions after irradiation with Nd:YAG laser and application of topical fluoride. One-hundred and twenty dentin samples obtained from bovine incisors were used. All samples were submitted to erosive cycles with citric acid solution. After 10 days of acid challenges, lesions became visible and OCT readouts were performed on day 01 (before the first acid challenge, on day 05, day 10, day 15, day 17 and day 20 The OCT images generated made it possible to measure the amount of tooth tissue loss over the 20 days of erosive cycle, before and after treatments, and to monitor early dentin demineralization progression. After statistical analysis, the fluoride group was observed to be the one that showed smaller loss of tissue over time. The OCT technique is promising for diagnosing and monitoring erosive lesion damage; however, further in vitro and in vivo research is needed to improve its use (Figure 12).

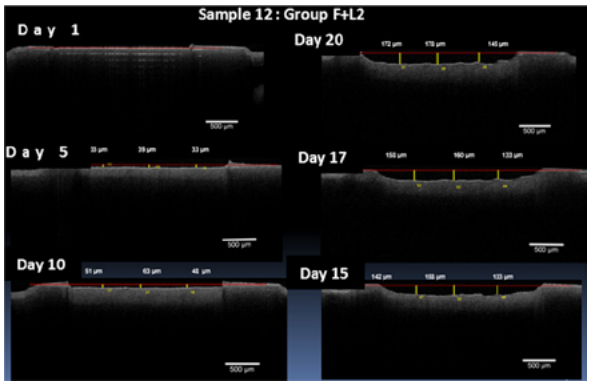

Figure 12: Microspheres and carbomer gel 1.0% (w/w), (a) sphere above the carbomer gel and (b) sphere within the carbomer gel.

Studies regarding the detection of flow are also being carried in the laboratory. Speckle, a form of coherent noise present in OCT, was shown to hold a time-dependent relation with regions of flow in the sample being imaged , and has been used to generate maps of such regions. A microfluidic volumetric flow determination using optical coherence tomography speckle was done. We propose a simple approach to the autocorrelation of OCT signal to enable volumetric flow rate differentiation, based on decorrelation time. Our results show that this technique could distinguish flows separated by 3 ul/min, limited by the acquisition speed of the system. We further perform a B-scan of gradient flow inside a microchannel, enabling the visualization of the drag effect on the walls (figure 13).

Laser Speckle Contrast Imaging (LSCI) is a technique proposed to assess the microvas-

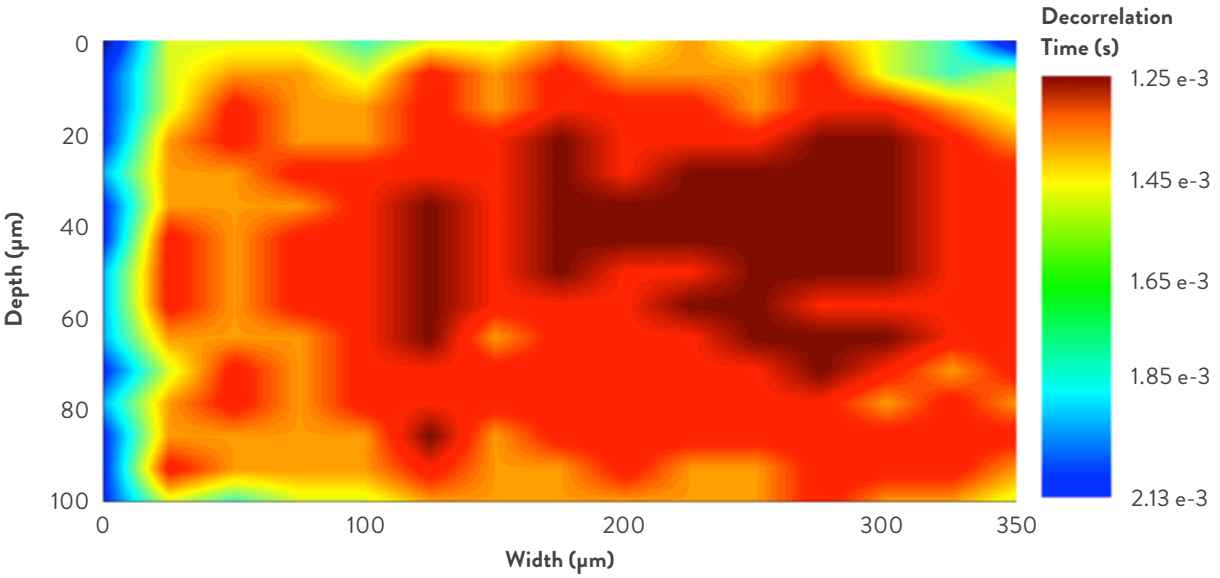

Fig 13 - Decorrelation time calculated for several points inside the microchannel while milk is pumped at 5ul/min. It functions as a B-scan of flow gradient inside the microchannel

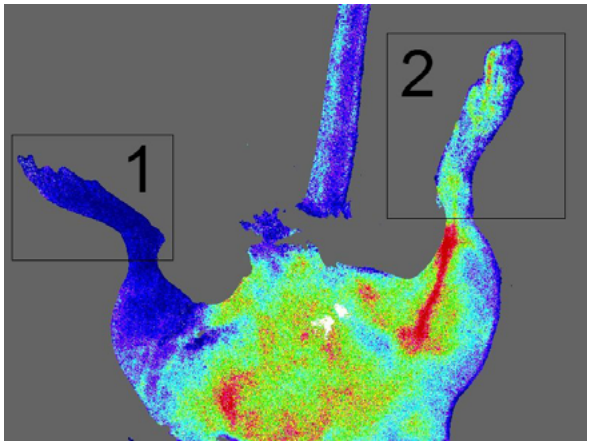

Figure 14: Typical mapping of blood flow from a C57BL/6 mouse produced via Laser speckle contrast imaging. Ischemic hindlimb in region (1) and control in region (2). Color code: blue meaning low flow to red meaning high flow.

cular function. Briefly, a low power (typically 50 mW), non-collimated laser radiation, frequently in the range from 635 nm to 780 nm, illuminates the skin. Scattered photons from static and moving (mainly red) blood cells in the microvascular plexus are collected by a CCD or a CMOS camera during a selected exposure time. The captured image presents a granular pattern, known as speckle pattern, due to interferences of the scattered radiation. The pattern changes with the movement of the red blood cells. The differences in the statistics of speckle patterns from static and moving structures are explored to compute a quantity related to the skin blood flow (SBF). A sequence of images is captured , and each frame is processed producing a mapping of blood flow in the investigated region. A region of interest (ROI) can be selected to compute a regional (into the ROI) blood flow. The result is a time series of SBF values. This spatial processing methodology allows high sampling rate (typically in the order of 25 frames/s), detecting rapid changes of flow. As a result of the non-contact feature of the LSCI system, any body movement of the target generally interferes in the measurement. This fact may restrict the use of the LSCI system to monitor the blood flow from anesthetized mice due to breathing movements. In attempt to correct the baseline of a signal with peaks, the background signal of each register was estimated using the MATLAB function msbackadj. Baseline tracking and correction is a common problem in DNA sequencing. Automated DNA sequencing is a well established technique. In this case, the accurate identification of a DNA sequence depends on the correction of the baseline of the chromatographic signal. The raw chromatogram generally presents a slowly varying baseline. For DNA sequencing, the correction of the baseline is necessary in order to establish a trustable reference of the background signal to further processing. In this case, the corrected data is the raw data minus the estimated baseline signal. Here (blood flow measurement, the estimated baseline is the useful signal. The raw data are used only to estimate the background signal. The measured SBF signal from mice hindlimbs via LSCI, Fig. 14, is corrupted by respiratory movements. The recovery of a SBF signal corrupted by artefacts from breathing is feasible, allowing more accurate measurements, Fig. 15.

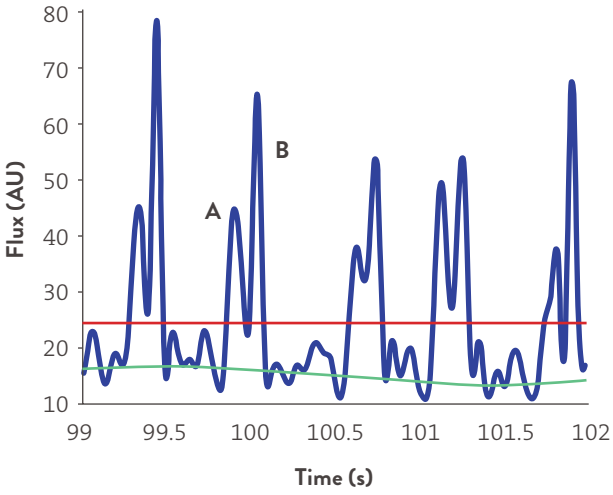

Figure 15: Raw register of blood flow from a control hindlimb during five minutes (blue), the corresponding mean value (red) and the estimated background signal (green). The measured flow is corrupted by respiratory movements: (A) inspiratory and (B) expiratory.

As a facility that has access to radioactive and nuclear materials, research and development

of lasers application in such area is an opportunity not easily found elsewhere.

Radioactive waste management poses a challenging and costly task. The possibility of decontaminate materials that present radioactive surface contamination helps in diminishing the required volume of the waste storages and at the same time allows the recycling of the material, which, frequently, has an high market value, such as copper, stainless steel and lead. Studies decontamination through laser ablation achieved 90% of activity reduction for stainless steel, and 60% for lead, pointing that this process needs to be further studied. Figure Figure 16 shows a scanning electron microscope image of a lead sample, before (left) and after (right) the laser irradiation.

integrity. The functionality demonstration of the detector has been achieved already; nonetheless more studies are being carried out to improve the process.

Laboratory of Environmental Laser Applications (LEAL) began its activities at IPEN in 1999 with the implementation of the first lidar system for tropospheric monitoring in Brazil. Lidars, also known as laser radars, are meant to profile the atmosphere with high temporal and spatial resolution of particles and gases and are import important instruments for pollution monitoring, atmospheric dynamics studies, nuclear safety surveillance and waste management control. Up to date, there are four systems developed/deployed by IPEN for several purposes. The earlier system is lab fixed with 7 channels which operates

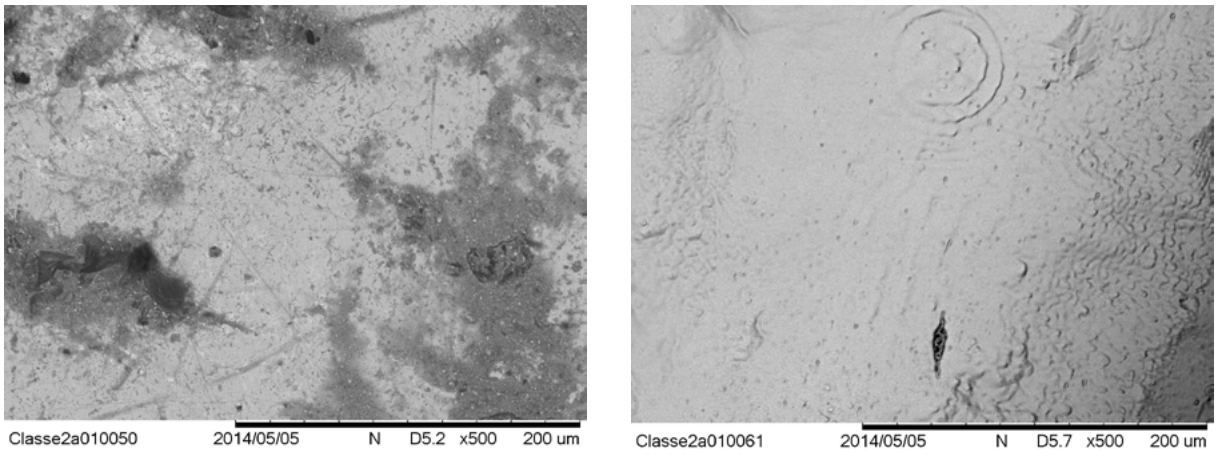

Fig. 16. Scanning electron microscope image of a lead sample, before(left) and after (right) the laser.

Another development being carried is the development of the deposition process of a thin layer film of boron by lasers aiming to develop a low cost and portable neutron detector. Boron has one of the highest evaporation temperatures among the chemical elements; furthermore, the boron deposition needs to occur on the surface of a semiconductor detector, thus discarding electron beams techniques, which could damage the detector

by the principles of Rayleigh, Mie and Raman scattering. This system has been operational since 2000 and has produced many results on aerosol long range transport, atmospheric dynamics and hydrological cycles and acted as a teaching tool has produced data to support several graduation thesis (Figure 17).

A second transportable system installed at LEAL has been performing many experiments

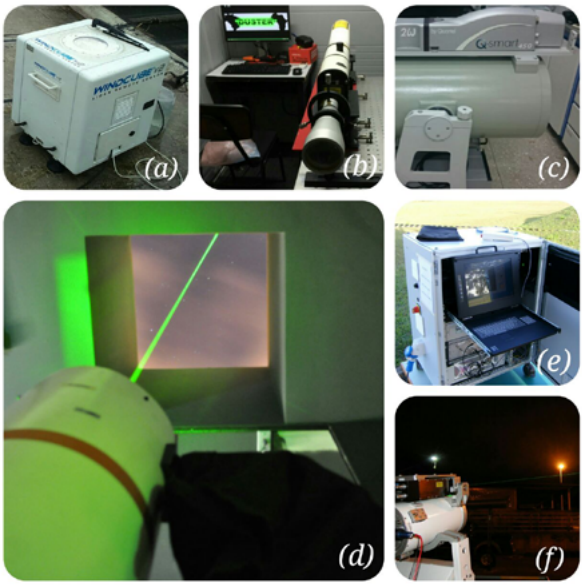

Figure 17. IPEN's Lidar systems for aerosol, trace gases and wind profiling.

all over the country supporting important state and federal projects. A tracking system was deployed in Cubatão in 2012 and active in pollution monitoring and dispersion studies in a heavily dense environment as Cubatão surrounded by oil and cement mills and a refinery, nowadays CETESB, the state environmental agency, is performing probe studies in identifying pollution sources with technique (Figure 18).

In 2014, LEAL started developing in-line systems for CO_2 monitoring in sequestration sites in collaboration with PETROBRAS and UNESP by the implementation of techniques such as CRDS (Cavity Ring Down Spectroscopy) and the use of quantum cascade laser technology.

LEAL is at the present in the coordination of LALINET (Latin American Lidar Network) aiming at local and regional network expansion, which opened the opportunity to set a system in Natal, in collaboration with the UFRN and University of Granada, Spain. This system is a 3-channel polarization sensitive laser system which grants the possibility of inferring particle shape and source and its main objective is to study Saharan dust transport over the Atlantic and its influence in our continent.

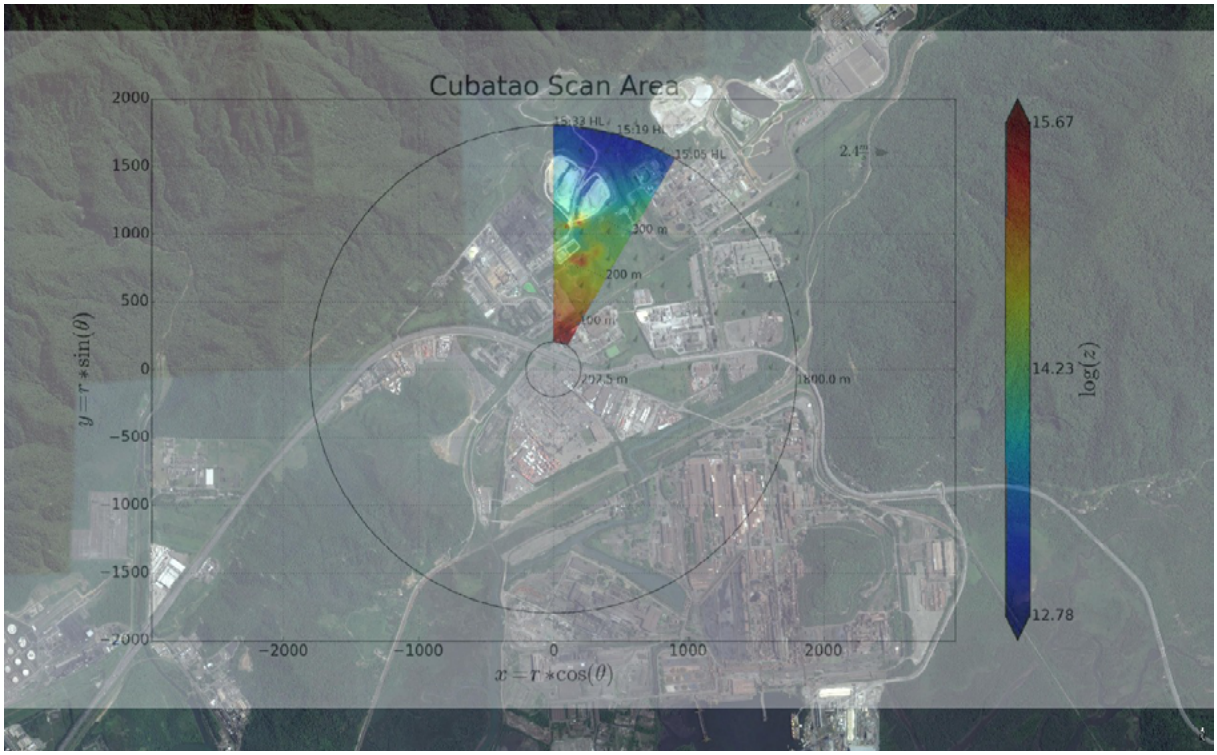

Figure 18. Industrial site mapping with MSP-III Scanning Lidar.

CLA is also involved in Operation and optimization of the TW peak power laser and applications. High power ultrashort pulses lasers based on CPA (Chirped Pulse Amplification) technologies allow the study, in conventional laboratory, of phenomena that only 15 years ago were restricted to national laboratories with annual budgets amounting to billions of dollars. In the Center for Lasers and Applications at IPEN, a hybrid Ti:Sapphire/Cr:LiSAF TW peak power laser system is under continuous development. A flashlamp pumping cavity for a Cr:LiSAF rod gain medium was developed and built, aiming to minimize the thermal load on the Cr:LiSAF crystal by the use of absorption filters between the lamps and the gain medium, allowing the amplification of ultrashort pulses to the terawatt peak power region at high repetition rates. The pumping cavity was initially used in a laser configuration, and generated 60 μs pulses with energy up to 2.8 J, with an average power of 30 W at 15 Hz repetition rate, the highest reported to date. The utilization of the pumping cavity in a hybrid Ti:Sapphire/Cr:LiSAF CPA configuration produced 60 fs pulses with 30 mJ of energy at 5 Hz repetition rate, reaching 0.5 TW of peak power, the highest in the southern hemisphere. Among other applications, these pulses can be focused to relativistic intensities to accelerate electrons up to MeV energies. Our laboratory also has another amplified laser system capable of generating up to 800 μJ, 25 fs pulses or 300 μJ, 5 fs pulses. Even at lower peak powers, the pulses very short duration generates nonlinear phenomena, particularly those initiated by multiphotonic and tunneling processes that generate free electrons.

Ultrashort pulses were utilized to ablate and machine technological materials with precision on the micrometer scales with negligible heat affected zones, and to study how laser created defects (color centers, vacancies) affect the ablation dynamics in various material such as metals and dielectrics. As a secondary effect of the ablation, shockwaves propagate into the substrate, generating extreme temperatures and pressures that can induce phase transitions; these phase transitions were studied in graphite, in which many allotropes were crated, including nanodiamonds. The nonthermal ablation was also used to remove necrosed material from burned animals and its effects on the tissue regeneration are under investigation.

The ablation of solids by ultrashort pulses is due to a Coulomb explosion following the ejection of surface electrons accelerated by the laser electric field, or by a phase explosion resulting from a high density of free electrons generated by avalanche ionization. The pulses have very brief duration, shorter than the typical phonon period, mainly heat the electrons and the explosions that remove material occur after the pulse has finished, with minimal material heating. The avalanche occurs when seed electrons, either already present in metals or created by tunneling or multiphoton ionization in other materials, are accelerated by the ultrashort pulse electric field into a quivering motion and generate more free electrons by impact ionization in an exponential growth process that is almost independent of the material being irradiated. The high intensities reached by ultrashort pulses easily induce the nonlinear phenomena that create the initial free electrons, making these pulses efficient tools to etch any kind of material. Due to this nonselective mechanism, the only parameter that must be known to etch a material with ultrashort pulses is its ablation threshold fluence, F_{th}. This ablation threshold derives from the material atoms bonding energies, electronic density and its ionizing energies, which depend on the pres-

ence of dopants, impurities or other defects. As a consequence of the defects presence, the seed electrons are created more easily and the avalanche ones are freed at lower impact energies, decreasing the F_{th} value. These defects can be created by ultrashort laser pulses , and in this case the modifications induced by a pulse modify the F_{th} value for the following pulses, until the defects density reaches saturation and F_{th} stabilizes at a constant value. These cumulative phenomena are known as incubation effects, and the ablation threshold fluency modifications caused by them must be considered when machining a material. A few years ago, we introduced a simple experimental technique, denominated D-Scan (Diagonal Scan), to quickly measure the ultrashort pulses ablation threshold of a solid sample. Recently, we modified this technique to allow the ablation threshold measurement for an arbitrary pulse superposition , and the consequently determination of the incubation effects. Knowing the ablation threshold for the superposition of multiple pulses is important when machining samples with ultrashort pulses, in which the sample displacement speed and laser repetition rate play an important role in setting the pulses overlap, and determine the morphology and quality of the structures etched. Our technique presents advantages over the traditional one due to its speed and also for reproducing the machining conditions more closely. Using the results obtained for the superposition of many pulses, new methods were developed to etch structures in the surfaces of technological materials minimizing the material modifications on the neighborhood of the etched regions.

Using the D-Scan, we have determined the ablation threshold of many materials, including glasses, metals, graphite and ceramics, among others. The ablation threshold dependence on the pulses superposition is an important parameter when machining these materials to create microstructures such as microfluidic and micro opto-fluidic circuits that are being developed and built at the Center for Lasers and Applications at IPEN. These parameters were used to investigate the influence of metals electron mobility and thermal conductivity on the ablation dynamics, the glasses ablation mechanism dependence on the pulse duration, and to texturize mechanical tools to improve their performance and reduce wear, and to promote selective ablation.

An interferometric system to maintain the laser focal point on the surface of a material being processed is under development. This system is based on the ultrashort pulses large bandwidth, and will improve the quality of the machining.

During the ablation by ultrashort pulses, the explosive material removal creates shockwaves that propagate into the substrate under irradiation. These shockwaves, besides promoting a local increase in the pressure, also rise the temperature in a propagating submicron layer. These conditions can be extreme and highly localized, due to the violent explosion resulting from the ultrashort pulses high intensity, and promote modifications in the substrate. We have demonstrated that the ablation originated shockwaves in amorphous graphite can change the hybridization of the carbon bonds from sp^2 to sp^3, increasing the order of the crystalline array, cumulatively creating different allotropes including nanodiamonds. Figure 19a shows a High Resolution Electron Diffraction of the diamond-like phase, and Fig. 19b shows the same analysis of the initial polycrystalline graphite (PG) substrate; Fig. 19c presents a High Resolution Electron Micrography of the laser created structure with the characteristic 0.205 nm d-spacing of the diamond phase evidenced by the zoom

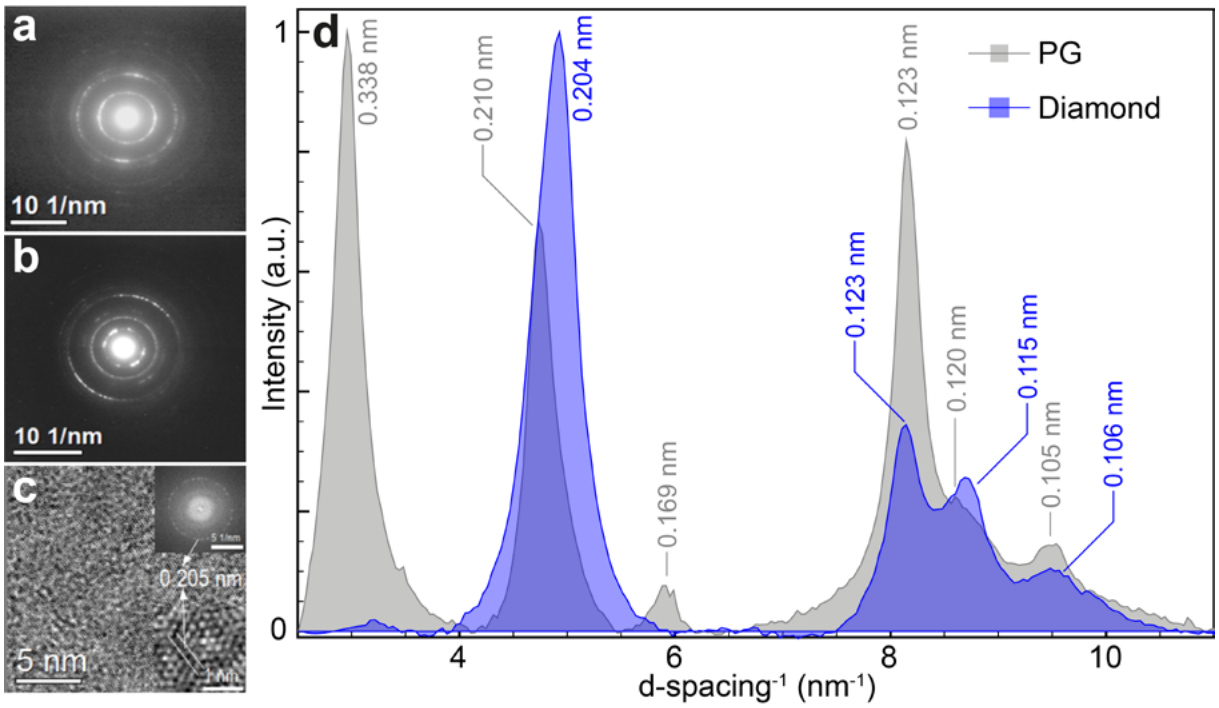

Figure 19 - High Resolution Electron Diffraction of the (a) diamond-like phase and (b), its graphite precursor; (c) shows a HRTEM micrography of the laser created structure with the characteristic 0.205 nm d-spacing of the diamond phase; (d) exhibits the corresponding electron diffraction peaks as a function of the inverse of the d-spacing for the precursor graphite (gray spectrum) and diamond-like phase (blue spectrum).

of a small area shown in the bottom inset. Fig. 19d exhibits the corresponding electron diffraction peaks as a function of the inverse of the d-spacing for the polycrystalline graphite (PG, gray spectrum) and diamond-like phase (blue spectrum).

The ultrashort pulses ablation creates an ablation plume that leaves the substrate in a highly energetic state, atomizing their molecules and ionizing these atoms, which return to their ground state emitting its characteristic atomic lines. This, the emission spectrum can be used to analyze the elemental composition of the substrate. This technique is known as fs-LIBS (femtosecond-Laser Induced Breakdown Spectroscopy), and can be used in dissimilar materials with similar efficiencies due to the nonselective characteristic of the ultrashort pulses ablation. Taking advantage of this fact, we used the fs-LIBS technique to determine the diffusion of dental amalgam elements (Hg, Ag, Cu and Sn) into the surrounding tooth structures. Figure 20 shows fs-LIBS spectra of (a) the amalgam, evidencing the presence of the metallic components, (b) the amalgam/dentin interface, and (c) the dentin. The metals can be observed in the interface, but they are absent of the dentin 400 µm away from the interface. Our results showed that the metals diffuse on the dentin of both deciduous and

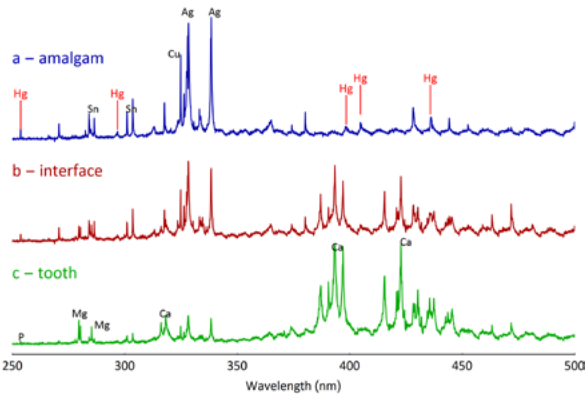

Figure 20. High Resolution Electron Diffraction of the (a) diamond-like phase and (b), its graphite precursor; (c) shows a HRTEM micrography of the laser created structure with the characteristic 0.205 nm d-spacing of the diamond phase; (d) exhibits the corresponding electron diffraction peaks as a function of the inverse of the d-spacing for the precursor graphite (gray spectrum) and diamond-like phase (blue spectrum).

permanent teeth by a couple of micrometers , and indicated that they diffuse by liquid transport processes, once different metals migrate by similar distances.

Ultrashort laser pulses were used to synthesize silver and gold nanoparticles controlling its size. Starting from colloidal salt solutions containing capping agents, these were illuminated by blue light that neutralizes the metallic atoms, which aggregate into clusters. The solutions containing the clusters were then irradiated by ultrashort pulses, which, through photolysis, break the clusters into smaller nanoparticles. We have found that controlling the pulse duration and its relative spectral phase is possible to determine the final nanoparticles average size and its dispersion. This method is now being improved to allow the synthesis of the nanoparticles controlling its geometry, enabling the production of spheres, rods, prims and on the nanoparticles shapes, thorough the use of an optical control feedback by analysis of the nanoparticles solution absorption spectra and a genetic algorithm. To use the genetic algorithm, nanoparticles solutions must be irradiated in a microfluidic circuit, which allows the use of small solution volumes that are modified and measured in a few seconds, making the use of a feedback loop practical. We have already shown the control of the nanoparticles size with this experimental scheme, and a patent application was submitted.

CLA is also involved in Generation of High Harmonics into the VUV and soft X-ray spectral regions as a complimentary light source for the new Brazilian Synchrotron. When a high intensity ultrashort pulse lasting tens of femtoseconds impinges on a gas at low pressure, electrons can be freed from its parent atoms by the leading of the pulses, and then be accelerated by the pulse carrier wave into a quivering motion, acquiring kinetic energy. When these electrons collide with the atom, their energy is released in the form of odd harmonics of the exciting field, and if the kinetic energy is sufficiently high, the harmonics can reach the UV and soft X-ray region, generating photons up to a few keV. In the High intensity ultrashort pulses laser laboratory, we are pursuing the generation of these harmonics into the region of the water window, around 2-4 nm, which are proposed to be used in high-resolution radiographies of living tissues. Using 785 nm, 650 μJ, 25 fs pulses at 4 kHz repetition rate pulses focused into an Argon jet inside a vacuum chamber, we generated harmonics in the 70-38 nm range (11th to 19th harmonics), into the XUV spectral region. These harmonics were spatially characterized using a double knife-edge experimental apparatus, revealing that the diameter (35-70 μm) and divergence (<1 mrad) of the HHG beams generated in our setup are similar to those commonly observed in synchrotron beams in the VUV-EUV spectrum, which usually have ~100 μm diameters at the sample and divergences around 1 mrad. Although ours beams have small energies, the measured parameters define beams that can be used as complimentary light sources to the Sirius, the new Brazilian Synchrotron, in the VUV spectral region, with different temporal resolutions. Our experimental apparatus is constantly being improved , and the generation mechanisms are under study to allow us to generate more energetic photons and beams in the VUV and into the soft X-ray region.

Program Team

Research Staff

Dr. Anderson Zanardi de Freitas; Dr. Denise Maria Zezell; Dr. Eduardo Landulfo; Dr. Gessé Eduardo Calvo Nogueira; Dr. Izilda Marcia Ranieri; Dr. Laercio Gomes; Dr. Marcus Paulo Raele; Dr. Martha Simões Ribeiro; Dr. Niklaus Ursus Wetter; Dr. Nilson Dias Vieira Junior; Dr. Ricardo Elgul Samad; Dr. Sonia Licia Baldochi; Dr. Wagner de Rossi; Tech. Jose Tort Vidal; Tech. Marco Antonio Andrade; Tech. Marta de Jesus Silva; Tech. Paulo Cesar da Silva; Tech. Valdir de Oliveira; Suely Tavares Venancio.

Postdoctoral Fellows / Graduate Students / Undergraduate Students

Adriana Fontes; Aguinaldo Silva Garcez; Alessandra Baptista; Alessandro Francelino Nogueira; Alexander Hincapié Ramirez; Allan Bereczki; Ana Paula F. Moraes; Anderson Pimentel Damian; Andreia de Araujo Almeida; Antônio Arleques; Armando Valter Felicio Zuffi; Beate Santos Saegesser; Bruno Britto Chiomento; Caetano Padial Sabino; Carolina Benetti; Carolina Gouvêa de Souza Contatori; Cássia M.L. Beu; Cassio A. Lima; Claudia Bianchi Zamataro; Cristhiano da Costa Herrera; Cristiane Lassalvia Nascimento; Cristiane Miranda França; Cristine Calil Kores; Daisa L. Pereira; Daniela de Fátima Teixeira da Silva; Danilo Mariano da Silva; Débora Picanço Aureliano; Denilson de Camargo Mirim; Derly A. Dias; Diego Silvério da Silva; Elaine C. Araújo; Eliane G. Larroza; Fabio Cavalcanti; Fábio J.S. Lopes; Fabio Parra Sellera; Fabio Pogliani; Fernanda de Mendonça Macedo; Fernanda Viana Cabral; Gilberto André dos Santos Rocha; Gregori Arruda Moreira; Greice Barros de Lima; Guilherme Soares Lopes; Hélio Pires Julião Borges Coelho; Henrique de Souza Rodrigues Silva; Ilka Tiemy Kato; Izabel S. Andrade; Jedaías Teófilo Pereira Júnior; Joao Pedro Fonseca Paes; Jonatan J. Silva; José Ângelo Lauletta Lindoso; José Carlos Gonçalves Perez; Leandro Gusmão da Silva; Leonardo Vieira Costa; Lucas Aparecido dos Santos Ferreira; Lucas Ramos de Pretto; Lucia R. Teixeira; Luis Claudio Suzuki; Maira Franco de Andrade; Maitê Santiago Nilzen; Marcello M. Amaral; Marcia C. D. Moraes; Márcia T.A. Marques; Marcio André Prieto Aparício Lopez; Maria H. G. A. Salani; Mariella S. Gottardi; Mauricio da Silva Baptista; Merilyn Santos Ferreira; Michael Hamblin; Patrícia Alves Barbosa; Patricia Ferrini; Paulo Guanabara Júnior; Paulo Roberto Gonçalves Lima; Paulo Sérgio Fabris de Matos; Priscila Costa; Rafael de Lima Denaldi; Regiane de Souza Pinto; Renato Araujo Prates; Renato Evangelista de Araujo; Sandro Martins de Alencar; Selly Sayuri Suzuki; Silvia Cristina Núñez; Tania Mateus Yoshimura; Tayná de Fátima Amorim Silva; Thaís Corrêa; Thiago da Silva Cordeiro; Walter M. Nakaema

Collaborators

Dr. Adriana Ramos de Miranda; Dr. Alessandro Melo Deana; Dr. Alexandre Ferreira Ramos; Dr. Alexandros Papayannis; Dr. Alvaro Bastidas; Dr. Amauri Oliveira; Dr. Anderson Stevens Leonidas Gomes; Dr. André Felipe Henriques Librantz; Dr. Antonieta Riquelme Silva; Dr. Ardson dos Santos Vianna Jr; Dr. Boris Barja; Dr. Carlos Lenz Cesar; Dr. Ceferino Lopez; Dr. Christiano de Matos; Dr. Cláudio Oller; Dr. Dário Santos Junior; Dr. Diego Silveiro da Silva; Dr.

Dimitri Geskus; Dr. Doina Nicolae; Dr. Eduardo Quel; Dr. Ernesto Jimenez Villar; Dr. Francisco Carlos Barbosa Maia; Dr. Frederico Antônio Genezini; Dr. Gelsomina Pappallardo; Dr. Helen Pask; Dr. Henrique Barbosa; Dr. Igor Veselovskii; Dr. Jean Jacques Zondy; Dr. Jefferson Bettini; Dr. José Eduardo Krieger; Dr. Juan Calos Antuña Marrero; Dr. Juan Luis Guerrero-Rascado; Dr. Judd Ellsworth Welton; Dr. Judith Hoelzemann; Dr. Julia Maria Giehl; Dr. Juliane C. Campos; Dr. Julio C. B. Ferreira; Dr. Júlio Meneghini; Dr. Lilia Coronato Courrol; Dr. Lucas Alados-Arboledas; Dr. Luciana Reyes Pires Kassab; Dr. Luciano Bachmann; Dr. Márcio A. C. Ribeiro; Dr. Maria Cristina Chavantes; Dr. Maria de Fátima Andrade; Dr. Maria Paulete Jorge; Dr. Narcizo Marques Souza-Neto; Dr. Neusa Paes Leme; Dr. Pablo Ristori; Dr. Patricia Aparecida da Ana; Dr. Paulo Artaxo; Dr. Philippe Delaporte; Dr. Raul de Oliveira Freitas; Dr. Réal Vallé; Dr. Ricardo Forno; Dr. Roberto Guardani; Dr. Rui Mário da Silva Vilar; Dr. Stuart D. Jackson; Dr. Tárcio Almeida Vieira; Dr. Telma M. T. Zorn; Dr. Volker Freudenthaler